Available online at www.sciencedirect.com
ScienceDirect
Remote Sensing of Environment 107 (2007) 312–321
Remote Sensing of Environment
www.elsevier.com/locate/rse

# Retrieving forest background reflectance in a boreal region from Multi-angle Imaging SpectroRadiometer (MISR) data

Francis Canisius *, Jing M. Chen

*Department of Geography, University of Toronto, 100 St. George St., Room 5047, Toronto, Ontario, Canada M5S 3G3*

Received 26 January 2006; received in revised form 7 July 2006; accepted 31 July 2006

**Abstract**

Studies of the bidirectional behavior of forest canopy have shown that the total reflectance of a forest canopy is the combination of illuminated and shaded components of the tree crown as well as the background. In this study, we estimate the background portion from the bidirectional reflection observed by Multi-angle Imaging SpectroRadiometer (MISR) instrument which scans the earth in nine different view angles in an oblique plane relative to the sun. The nadir and 60° forward directions of the MISR images were used to derive the reflectivity of the forest background based on the probabilities of viewing the illuminated tree crown and background on those view angles. The probabilities were estimated using the Four-Scale model. In the study, background reflectivity mosaic images in red and NIR wavelengths covering the BOREAS region during winter and spring seasons were obtained. The mosaic images of winter show high background reflectivity in both wavelengths, and in most of the areas the reflectivity was more than 0.3. In mosaic images of spring the spatial variations in the background reflectivity were considerable. The seasonal changes in the background reflectivity were also studied with multi temporal MISR data, and a similarity in the temporal pattern was found between the retrieved forest background reflectivity and grass land reflectance. These spatial and temporal patterns of the background component retrieved from MISR would be critically important in retrieving the biophysical parameters of vegetation and in ecosystem modeling.


*Keywords:* Multi-angle remote sensing; Forest background reflectance; MISR; BOREAS

## 1. Introduction

Understanding the global climate changes and developing strategies for sustainable use of our environmental resources are major scientific and political challenges (Hese et al., 2005). Vegetation response to the level of $CO_2$ and other greenhouse gases in the atmosphere is significant in climate change modeling (Field et al., 2003; Peddle et al., 1999; Potter et al., 2003). Carbon fluxes between atmosphere and biosphere have been estimated using biosphere models (Chen et al., 2003a; Hese et al., 2005) which require biophysical information of vegetation such as biomass, LAI and NPP (Chen et al., 2003b). Remote sensing has been demonstrated to have wide applicability in analyzing biophysical parameters of vegetation (Treitz & Howarth, 1999). However, traditional methods such as NDVI for deriving these variables from remotely sensed data have been inconsistent and unsatisfactory due to factors such as the confounding influence of background reflectance and canopy structure on the overall pixel reflectance (Peddle et al., 1999).

Multi-angle remote sensing delivers additional information about vegetation in terms of directional characteristics related to its vertical structure (Diner et al., 1999; Hese et al., 2005; Leblanc et al., 1999; Verstraete et al., 1996), and there have been a number of studies carried out to extract information on optical properties and structure of vegetation from the multi-angle data (Chen et al., 2003b; Cierniewski et al., 2004; Deering et al., 1999; Gao et al., 2003; Rautiainen et al., 2004; Sandmeier & Deering, 1999; White et al., 2001; Zhang et al., 2002b,a). Sandmeier and Deering (1999) and Zhang et al. (2002b,a) introduced angular indices of forest canopy structure to characterize biome signatures and used these indices to classify land cover types. Hu et al. (2003), Knyazikhin et al. (1998) and Chen et al. (2003b) proposed methods for deriving the leaf area

* Corresponding author.
*E-mail address:* franciscanisius@yahoo.com (F. Canisius).

0034-4257/$ - see front matter © 2006 Elsevier Inc. All rights reserved.
doi:10.1016/j.rse.2006.07.023

index (LAI) and the fraction of photosynthetically active radiation (FPAR) absorbed by the canopy using multi-angle data. Leblanc et al. (2005) and Chen et al. (2005) developed an angular index based on hotspot and darkspot reflectances for mapping the foliage clumping index from multi-angle measurements. Gobron et al. (2002) demonstrated the potential to map surface cover heterogeneity from multi-angle data at the subpixel scale resolution. Nolin (2004) retrieved the forest cover density over snow and Chopping et al. (2003) studied the canopy attributes of desert grassland using multi-angle imagery. All these studies demonstrate the large information content of multi-angle remote sensing. However, the ability of multi-angle remote sensing for retrieving vegetation background optical properties has not been systematically investigated.

Based on the field measurements (Peltoniemi et al., 2005; Pradhan, 2001) the reflectance values of the backgrounds such as soil, grass, moss, shrub, litter, lichen and their mixture vary as per their physical and chemical properties. Gemmell (2000) illustrated that the variations in the background reflectance would prevent the retrieval of forest structural characteristics at low to intermediate covers unless these variations can be taken into account. Field measurements of the background reflectance involve significant technical and logistical challenges, including complex spatial distributions of forest understory features and variable illumination conditions, as well as the demands of field measurements in relatively remote field sites (Gemmell, 2000). In this study, we examine the feasibility of using multi-angle remote sensing to determine the optical properties of the vegetation background (soil/moss/grass/shrub in forests). The Four-Scale model (Chen & Leblanc, 1997; Leblanc et al., 1999), which uses geometric-optical and radiative transfer theories (Chen & Leblanc, 2001) to calculate the angular reflectance of vegetation, was used to examine the feasibility of determining the background information given two viewing geometries with an inversion approach.

## 2. Methodology

### 2.1. Retrieval of background reflectivity

The total spectral reflectance ($R$) of a pixel results from the reflection of the scene components. In the case of a forest canopy, the reflectance is calculated by associating reflectivities of the sunlit and shaded tree crowns ($R_T$ and $R_{ZT}$) and background ($R_G$ and $R_{ZG}$) to the corresponding four probabilities of these scene components viewed by the sensor (Chen & Leblanc, 1997; Li & Strahler, 1985):

$$R = P_T \times R_T + P_G \times R_G + Z_T \times R_{ZT} + Z_G \times R_{ZG} \quad (1)$$

where $P_T$ and $P_G$ are the probabilities of viewing illuminated tree crown and background, respectively, and $Z_T$ and $Z_G$ are the probabilities of seeing shaded crown and background, respectively. Here the term background indicates all the materials below the forest canopy including rock, soil, leaf litter, lichen, moss, grass, shrub and snow or their mixture which are visible from above (Gemmell, 2000).

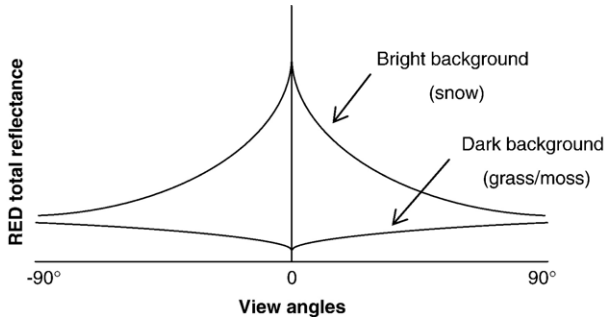


Fig. 1. The variation of the total reflectance of a forest canopy in a Red band with view zenith angle on the perpendicular plane for two contrasting background types.

The contribution of the background to the total reflectance changes with view angle as the probability of viewing the background decreases with increasing view zenith angle. Fig. 1 shows the influence of the background on the total bidirectional reflectance of a coniferous forest canopy at different view angles on a perpendicular plane (defined by the sensor and the ground target in a vertical plane) relative to the sun's azimuth. In this conceptual sketch, it is assumed that the sun is at a fixed angle and the total reflectance from a vegetated surface consisting of vegetation and the background varies with view angle. This variation occurs due to the contributions of the vegetation and the background varies with view angle. At nadir, the background contribution is the largest, while at the largest view zenith angle, the contribution of the vegetation is the largest. If the background is snow with a higher reflectivity than that of the overlying forest canopy in a red band, as an example, its contribution to the total reflectance would be high in the nadir direction, and the contribution would reduce rapidly with view zenith angle as the probability of viewing the background decreases. Assuming that the reflected radiance from the canopy changes little on the perpendicular plane, the total reflectance would then decrease with increasing view zenith angle. On the other hand, grass or moss with a reflectivity that is similar to or lower than the forest canopy would have the opposite effect on the total reflectance as the view zenith angle increases. However, in reality the reflected radiance from the canopy alone would change significantly across the zenith angle range even on the perpendicular plane on which the canopy shadow fraction viewed by the sensor changes significantly, and this issue can be effectively tackled by a geometrical optical model (Section 2.2).

Though the satellite orbit falls on an oblique plane, the difference in bidirectional reflectance due to the influence of the background could be observed by cameras viewing the surface on a plane that is not too close to the principal plane. By using the observed reflectance at nadir and at an angle in the forward direction (dark spot side) one can derive the background reflectivity ($R_G$). Assuming the background reflection is Lambertian, i.e., the reflectivity does not change with angle of observation, the reflectance at nadir ($n$) and another zenith angle ($a$) can be expressed using Eqs. (2) and (3).

$$R_n = P_{Tn} \times R_T + P_{Gn} \times R_G + Z_{Tn} \times R_{ZT} + Z_{Gn} \times R_{ZG} \quad (2)$$

$$R_a = P_{Ta} \times R_T + P_{Ga} \times R_G + Z_{Ta} \times R_{ZT} + Z_{Ga} \times R_{ZG} \quad (3)$$

Solving the Eqs. (2) and (3), with the assumption that the shaded reflectivities are comparatively small ($R_{ZT}=R_{ZG}=R_Z$), the background reflectivity $R_G$ can be expressed as:

$$R_G = \frac{R_a - P_{Ta}/P_{Tn} \times R_n + R_Z(P_{Ta}/P_{Tn} - P_{Ta}/P_{Tn} \times P_{Gn} + P_{Ga} - 1)}{P_{Ga} - P_{Ta}/P_{Tn} \times P_{Gn}} \quad (4)$$

Using the Eq. (4), the background reflectivity ($R_G$) can be calculated based on the reflectances of a pixel in the nadir and angular directions, if the probabilities of viewing the illuminated tree crown ($P_T$) and the background ($P_G$) in nadir and the angular directions are known. Here the values 0.002 and 0.08 were given as shaded reflectivity ($R_Z$) for visible and near infrared wavelengths, respectively.

### 2.2. Estimating probabilities of viewing scene components

The Four-Scale model developed by Chen and Leblanc (1997) was used to calculate two basic probabilities $P_T$ and $P_G$ in the nadir and angular directions. This is a geometric optical model with a focus on the effects of forest canopy architecture at various scales on the angular variations of remote sensing reflectance. In the Four-Scale, trees are modeled as nonrandom discrete objects with internal structures such as branches and shoots. Trees are grouped in variable sizes determined by a Poisson process to simulate certain patchiness of a forest stand. Tree crowns have different geometric shapes for different forest types. For a conifer crown, there is a cone on top of a cylinder, and for a deciduous crown, it is a spheroid with variable vertical and horizontal dimensions. Each crown is treated as a complex medium in which shoots of coniferous or leaves of deciduous types can cast shadows on each other so that even on the sunlit side of the crown, shaded foliage could be observed by the sensor. The site parameters such as tree density and grouping index are also considered to compute the fraction of gaps that allows the solar beam to penetrate through the canopy or a view line to reach the background.

Although the Four-Scale model requires many input parameters, it remains a powerful tool as it can be run with fixed general parameters or with best estimates of the missing parameters but in the mean time, very detailed simulations can be made when measurements of most parameters are available (Leblanc et al., 1999). Therefore it is an appropriate tool for this study involving a large area with fixed general parameters. Based on Chen and Leblanc (1997), tree architectural parameters of coniferous and deciduous forest types in the study area (Table 1) are used as input to the Four-Scale model.

Other than the above fixed parameters for two main forest classes, several parameters such as leaf area index, solar zenith angle, view zenith angle and the relative azimuth angle between the sun and the viewer varied between pixels in the region. These parameters could be obtained from the satellite images. Running the Four-Scale model on a multi-angle image pixel by pixel is computationally impractical, and we therefore used the model to create look-up-tables (LUT) for image processing.

Table 1
Tree parameters for the Four-Scale model

| Four-scale model parameters | Coniferous | Deciduous |
|---|---|---|
| Number of trees per ha | 2000 | 1000 |
| Clumping index | 0.7 | 0.8 |
| Tree shape | Cone + cylinder | Spheroid |
| Stick height (trunk space) | 5 m | 10 m |
| Crown height | 15 m | 10 m |
| Radius of crown | 1 m | 2 m |

### 2.3. Four-Scale look-up-tables

Two LUTs for the coniferous forest and deciduous forest types, respectively, were developed using the Four-Scale model. As shown in the sample LUT (Table 2), each LUT provides the probabilities of viewing sunlit foliage ($P_T$) and background ($P_G$) components as a function of leaf area index (LAI), solar zenith angle (SZA), view zenith angle (VZA), and the relative azimuth angle between the sun and the viewer (PHI). Ranges of values, LAI from 0.1 to 10, SZA from 0° to 70°, PHI from 100° to 170° along with MISR VZA 0°, 25°, 45°, 60° and 70° were selected to reduce the length of the LUT.

In the sample LUT (Table 2) the factors influencing $P_T$ and $P_G$ and their importance to estimate $P_T$ and $P_G$ can be clearly seen. It is obvious, as foliage coverage (LAI) increases, $P_T$ increases and $P_G$ reduces. Due to the tree crown geometry, $P_T$ and $P_G$ change with view zenith angle, and $P_G$ is maximum in the nadir direction. As shown in Table 2, when the VZA changes from 45° to 60°, $P_T$ increases and $P_G$ decreases. When SZA changes from 30° to 40°, both $P_T$ and $P_G$ decrease as the shaded components increase with SZA. $P_T$ and $P_G$ are both low at high PHI values (forward scattering side) where the probabilities of observing the shaded components are high.

## 3. Study area

This study was conducted over the Boreal Ecosystem-Atmosphere Study (BOREAS) region located in Manitoba and Saskatchewan, Canada, where many optical and canopy architectural measurements were made by Canada Center for Remote Sensing (CCRS). This region is bounded between 49° to 59° North and 94° to 110° West covering the area around 1,000,000 km$^2$. The landmarks are the Hudson Bay located at the top left corner and the Winnipeg Lake at the bottom right. Coniferous forest is the dominant vegetation type representing more than 40% of the region and other land cover types are deciduous forest, mixed forest, crop land, shrub land, grass land, burnt area, barren land, and open water (Liu et al., 1999).

## 4. MISR data and processing

MISR, the Multi-angle Imaging SpectroRadiometer, is the one of five instruments mounted on Terra spacecraft. The spacecraft flies in a sun-synchronous 705 km descending polar orbit, so that it crosses the equator always at 10:30 am local time (Diner et al., 2002). The MISR instrument consists of nine pushbroom cameras arranged in different view angles relative to

Table 2
Sample LUT of coniferous forest

| LAI | VZA | SZA | PHI | $P_T$ | $P_G$ |
|---|---|---|---|---|---|
| ..... | ..... | ..... | ..... | ..... | ..... |
| 2.8 | 45 | 30 | 140 | 0.1809 | 0.1241 |
| 2.9 | 45 | 30 | 140 | 0.1824 | 0.1160 |
| 3 | 45 | 30 | 140 | 0.1837 | 0.1085 |
| 3.1 | 45 | 30 | 140 | 0.1850 | 0.1016 |
| 3.2 | 45 | 30 | 140 | 0.1861 | 0.0951 |
| 3.3 | 45 | 30 | 140 | 0.1872 | 0.0891 |
| 3.4 | 45 | 30 | 140 | 0.1882 | 0.0835 |
| ..... | ..... | ..... | ..... | ..... | ..... |
| 3.6 | 60 | 30 | 140 | 0.2044 | 0.0276 |
| 3.7 | 60 | 30 | 140 | 0.2045 | 0.0253 |
| ..... | ..... | ..... | ..... | ..... | ..... |
| 3.8 | 60 | 40 | 140 | 0.1530 | 0.0182 |
| 3.9 | 60 | 40 | 140 | 0.1531 | 0.0166 |
| ..... | ..... | ..... | ..... | ..... | ..... |
| 4.2 | 60 | 40 | 160 | 0.1472 | 0.0126 |
| 4.3 | 60 | 40 | 160 | 0.1472 | 0.0115 |
| 4.4 | 60 | 40 | 160 | 0.1471 | 0.0106 |
| ..... | ..... | ..... | ..... | ..... | ..... |

the earth's surface, and the along-track angles are 0° (nadir) for the An camera, and 26.1°, 45.6°, 60.0° and 70.5° forward and backward of nadir for the Af/Aa, Bf/Ba, Cf/Ca, and Df/Da cameras, respectively (Diner et al., 1998). Each camera uses four Charge-Coupled Device (CCD) line arrays in a single focal plane. The line arrays cover 360 km wide swath and provide four spectral bands in Blue, Green, Red and Near Infrared (NIR) that are centered at 443, 555, 670 and 865 nm, respectively (Jovanovic et al., 1998). The resolution of all four bands in nadir view and the red band at all nine angles is 275 m and the resolution of other bands is 1100 m (Diner et al., 2002). So the MISR instrument produces bidirectional multi-spectral images of the ground surface allowing the observation of a given pixel at nine viewing angles in an oblique plane relative to the sun (Fig. 2).

Calibrated MISR radiance images from multi-angle and multi-spectral cameras after radiometric and geometric corrections are available as the Level 1B2 georectified radiance product. MISR Level 2 products are resampled to 1100 m resolution and are screened for contamination from sources such as clouds, cloud shadows, sun glitter over water, topographically complex terrain, and topographically shadowed regions (Bothwell et al., 2002). The Level 2 products are bihemispherical and directional-hemispherical reflectance (albedo), bidirectional reflectance factor (BRF), BRF model parameters, leaf-area index and biome (Bothwell et al., 2002).

MISR Level 2 products used in the study are provided in the Space Oblique Mercator (SOM) projection in equal-sized blocks of an ellipsoidal surface defined by the World Geodetic System 1984 (WGS84). The block construct enables the co-registration of nine-angle, four-band images with a minimal waste of space and processing effort (Bothwell et al., 2002) and allows to stack all the blocks of an orbit into a single dataset. Parameters of a product are also stored in these stacked-block grid data structures.

An ENVI plug-in was developed to read the data stored in stack-block and compute background reflectivity ($R_G$) from nadir and angular BRF images. Other than the BRF images, Canada 2000 Landcover map (to select a LUT), and LUT parameters such as LAI, VZA, SZA and PHI (to select $P_T$ and $P_G$ from the LUT) are additional input layers to run the program. If LUT parameters are not available, it can be run with fixed general parameters. Though the MISR product contains LAI, occasionally it was not presented for all the pixels of the data, as a result the relationship between the Simple Ratio (SR) of near-infrared (NIR) and red reflectances and the MISR LAI product was developed during summer season for coniferous and deciduous forests separately and applied to the SR image to calculate LAI. VZA was fixed for a given MISR angular image. SZA was extracted directly from the MISR GEO product. PHI was calculated using Solar Azimuth Angle (SAA) and View Azimuth Angle (VAA) values that are also available in the MISR GEO product.

## 5. Results

### 5.1. Bidirectional reflectance of forest canopy

Fig. 3(a) and (b) show the bidirectional reflectance of coniferous and deciduous forests on an oblique plane observed by MISR in red and NIR wavelengths, respectively. The angular patterns of the reflectance curves show some influence of the hotspot and the dark spots in the forest (Chen & Leblanc, 1997), which are most pronounced on the principal plane and become less pronounced as the azimuthal difference between the principal plane and the observation plane increases. The observational plane in the case presented in Fig. 3(a) and (b) was about 45° from the principal solar plane, so only a hint of the hotspot appears on the curves. When two forest types are compared, the coniferous forest shows lower values in the red band in the forward scattering side and much smaller values in the NIR band. These differences may be due to (i) the more distinct conifer crown structure than deciduous crown structure, causing stronger shadows, and (ii) the effect of foliage on bidirectional reflectance as broadleaves have much larger scattering albedos (reflectivities plus transmissivities) than needleleaves in NIR wavelengths.

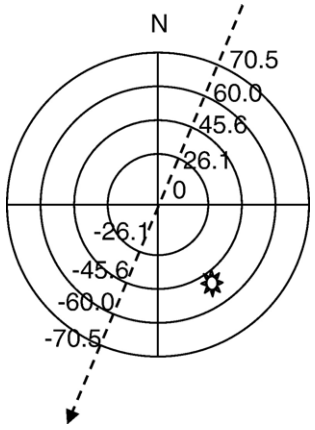


Fig. 2. Explanation of view angles.

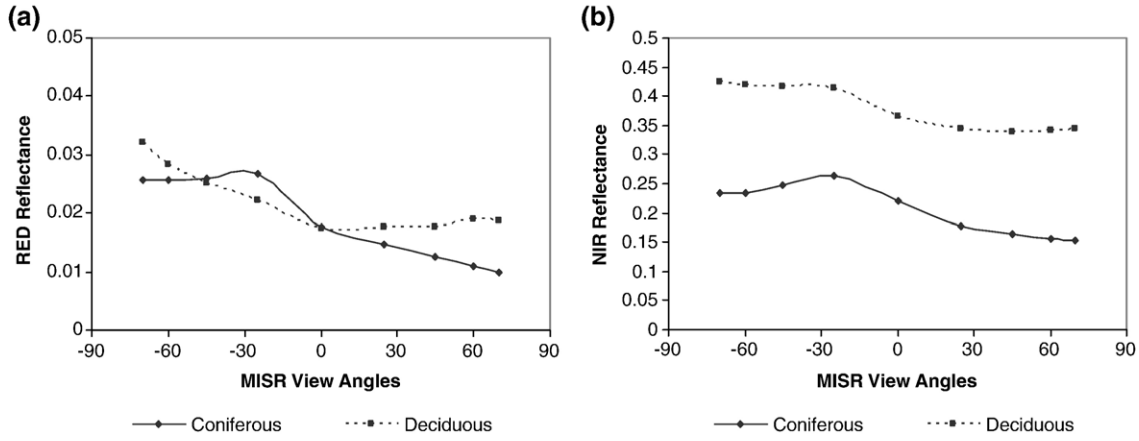


Fig. 3. Bidirectional reflectance of forest canopy as obtained by MISR on 08 July 2005. (a) Red and (b) NIR.

### 5.2. Seasonal changes in bidirectional reflection

When MISR observations are analyzed for different seasons, the influence of background on bidirectional reflectance as explained in the Methodology section (Fig. 1) can be discerned. As the MISR observation was made in this latitude range on an oblique plane about 45° from the perpendicular plane, the contribution of the forest canopy to the observed total reflectance may change greatly within the view angle range. Fig. 4(a) shows a pattern of the red bidirectional reflectance during the winter season where snow was the main background, causing a higher reflectance at nadir than at large view zenith angles as the probability of viewing the background decreased with increasing view zenith angle. Though coniferous forest is evergreen, there was a difference in the reflectance between early spring and summer seasons, i.e. the red reflectance (Fig. 4(a)) was low and NIR reflectance (Fig. 4(b)) was high in summer. This difference could be an indication of the background greening process. For the deciduous forest (Fig. 4(c)), the pattern of the red bidirectional reflectance during the winter is similar to that of the coniferous forest but with a broader peak near nadir as leafless canopies allowed easier penetrations of both the solar beam and the view line to the background than conifer canopies. Unlike coniferous pixels, the difference in the reflectances between early spring and summer seasons in both red (Fig. 4(c)) and NIR (Fig. 4(d)) were quite large for deciduous forest pixels, because

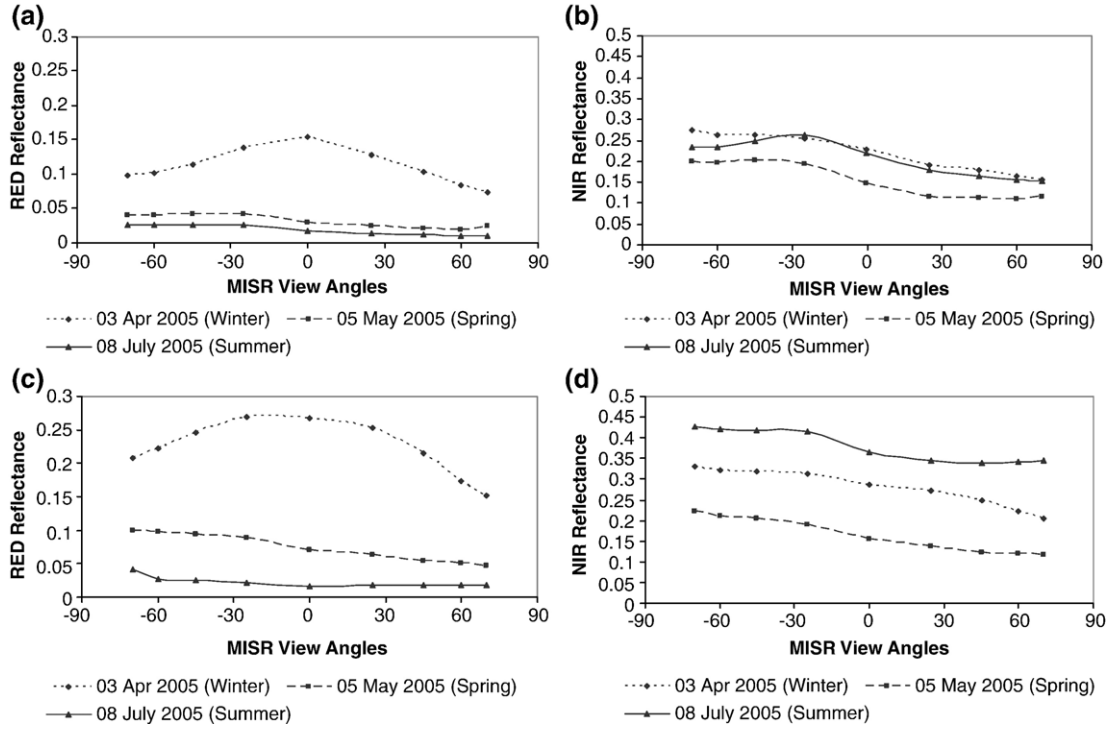


Fig. 4. Comparison of seasonal patterns of bidirectional reflectance observed by MISR. (a) coniferous forest in Red band, (b) coniferous forest in NIR band, (c) deciduous forest in Red band and (d) deciduous forest in NIR band.

of the growth of the new leaves in deciduous forests as well as the background vegetation.

### 5.3. Background reflectivity

After applying the LUTs to MISR images, the background reflectivity of the study area was mapped for several dates in 2000 (Fig. 5). Fig. 5(a) and (c) are mosaics of four background reflectivity images of 8 February 2000, 16 February 2000, 18 February 2000 and 16 March 2000 in the winter season in red and NIR, respectively. They show high background reflectivity values in both wavelengths, and in most area within the mosaics, the retrieved background reflectivity is more than 0.3. The mosaics of four background reflectivity images during spring (24 April 2005, 5 May 2005, 8 May 2005 and 16 May 2005) are shown in Fig. 5(b) and (d) for red and NIR, respectively, and spatial variations in the background reflectivity are quite apparent. The background reflectivities were high in the snow area in the northern belt, whereas they were low in most areas in the central part of the study region. Coniferous forests in the east side of the mosaics showed slightly brighter backgrounds (mostly moss) than other non-green areas. The deciduous forest in the south (no foliage in May) shows background reflectivity values similar to reflectances of bareland in both red and NIR.

### 5.4. Temporal variation of the background reflectivity

Rather than individual images, a time series of images track the changes in the background. To create time series information, 36 images that fall in 12 MISR paths over the study area were

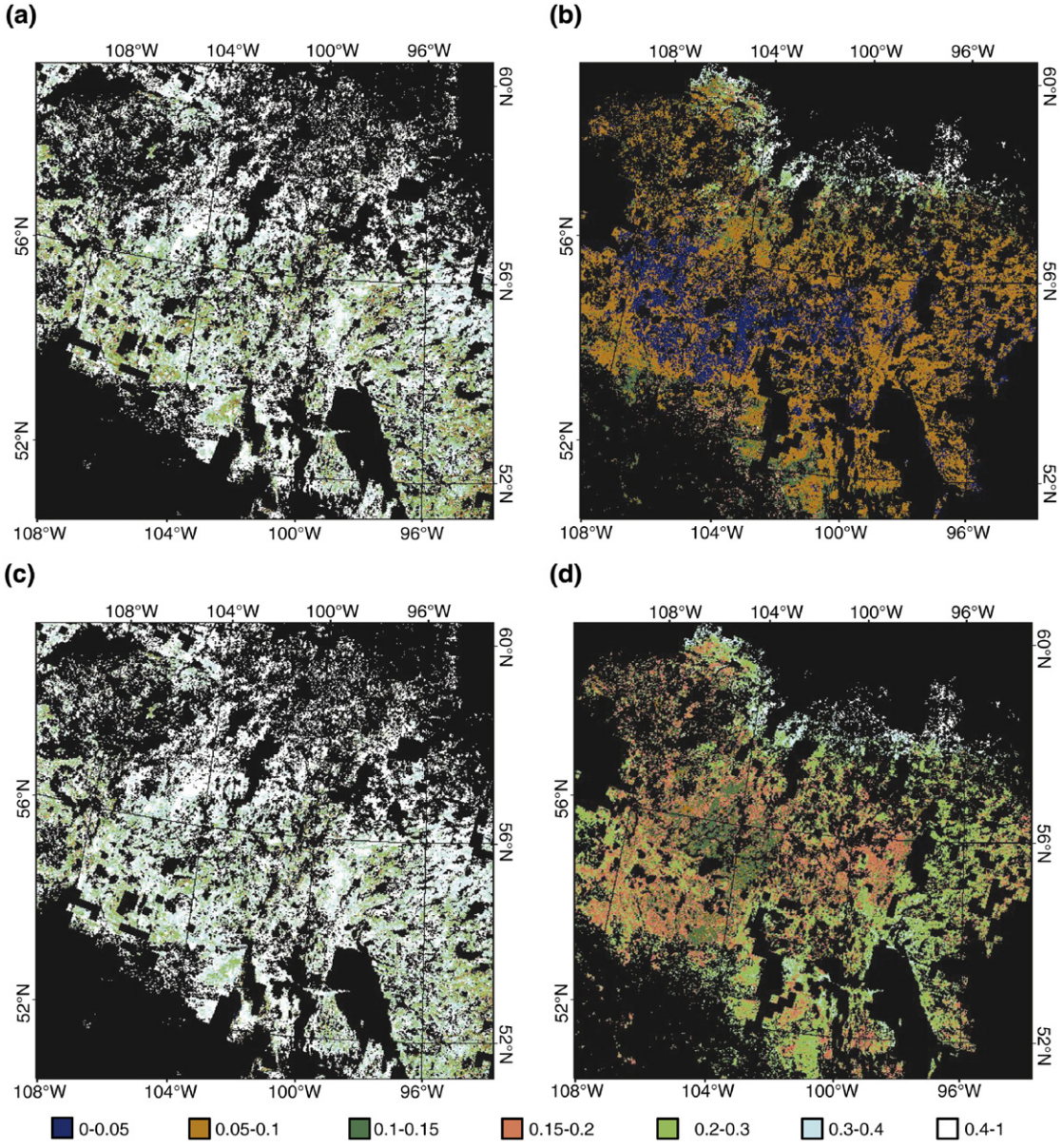


Fig. 5. Background reflectivity of forest area (a) Red band in winter (b) Red band in spring (c) NIR band in winter (d) NIR band in spring.

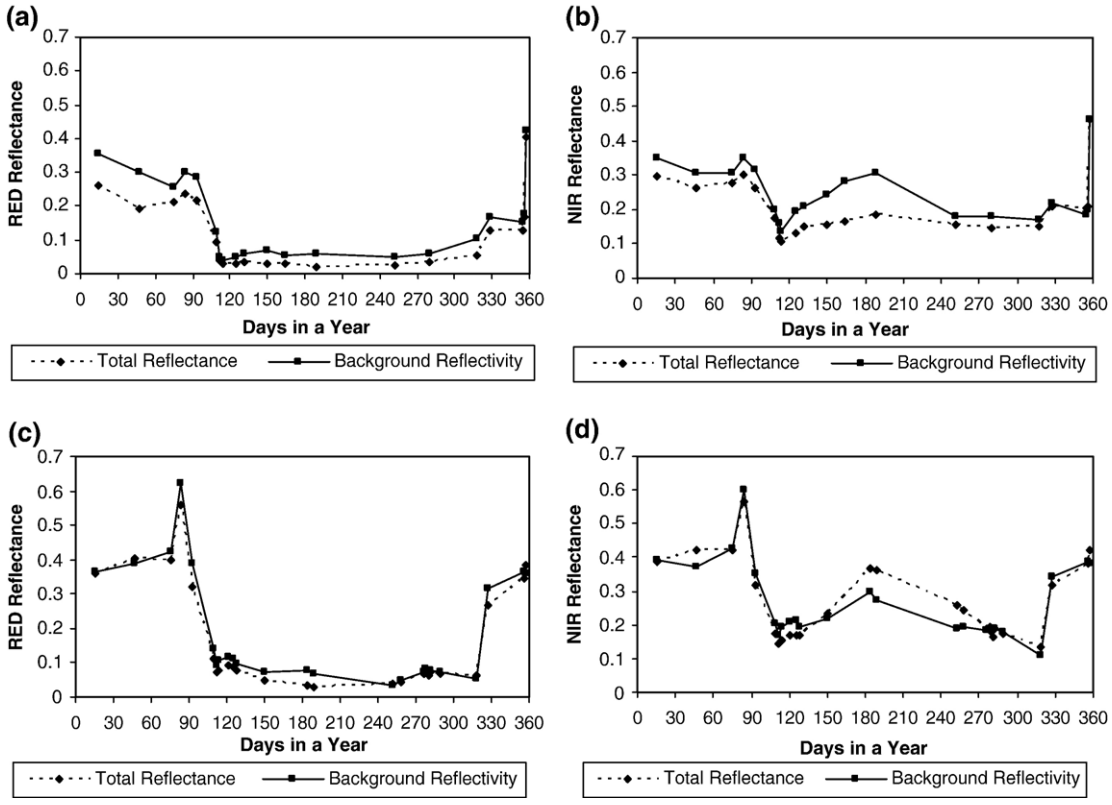


Fig. 6. Background reflectivity and its temporal changes of (a) coniferous forest in the Red band, (b) coniferous forest in the NIR band, (c) deciduous forest in the Red band (d) deciduous forest in the NIR band.

processed. Sample areas (more than 1000 pixels each) for coniferous and deciduous forests were selected over the study area to have as many points in time as possible to construct seasonal trajectories. Fig. 6 shows the total reflectance of the MISR images and the average of retrieved background reflectivity of these sample areas. In coniferous forests (Fig. 6(a) and (b)), the background reflectivity was consistently higher than the total reflectance. In winter, the background reflectivity was highest in both wavelengths but not as high as fresh snow. During spring and early summer the background reflectivity in NIR increased with the growing season. From these results, temporal variations in coniferous (evergreen) forests mostly due to the background can be clearly seen. In the case of deciduous forests, during winter, there were no large differences between the total reflectance and the retrieved background reflectivity. In summer, the background reflectivities in red and NIR showed similar growing patterns as the forest canopies, but they were lower than the total reflectance in the NIR band and higher than the total reflectance in the red band as expected.

### 5.5. Comparison of the background reflectivity with grassland

It is difficult to validate the results of the retrieved background reflectivity as the low resolution data was used in this study and

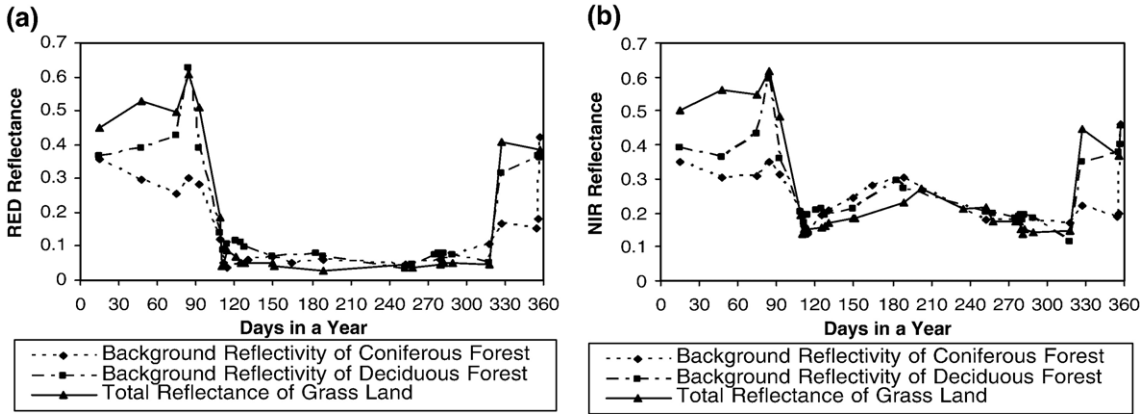


Fig. 7. Comparison of retrieved background reflectivity in coniferous and deciduous forests with open grassland reflectance in (a) Red and (b) NIR wavelengths.

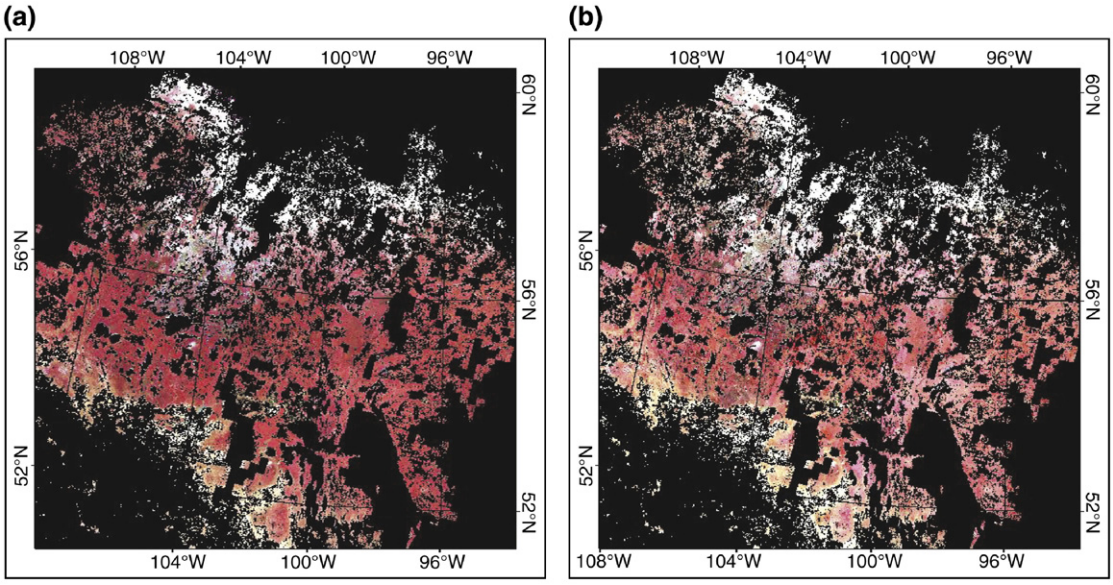


Fig. 8. RGB color composites of forest areas in spring. (a) NIR, Red and Green bands of MISR nadir reflectance data, and (b) NIR, Red and Green background reflectivities retrieved using MISR data.

the area coverage was very large. Systematic field measurements of background reflectivity are not yet available for a complete validation of our results. Therefore, as partial validation, the retrieved background reflectivity was compared with the reflectance of open grassland in the vicinity. Assuming that grassland reflectance and the background reflectivity in forests have similar seasonal variation patterns, the information contained in the MISR images for non-forest types can then be used to evaluate the performance of our algorithm for background information retrieval. It is very encouraging to us that the retrieved background reflectivities for both coniferous and deciduous forests follow similar seasonal trajectories as the reflectance of grassland (Fig. 7). The magnitudes in both red and NIR are similar in summer, indicating both grassland and the backgrounds follow similar greening and senescence patterns. In winter, the background reflectivities in forests are smaller than the grassland reflectance, suggesting that the background information retrieval in forests may be partly influenced by non-green materials in the canopy (trunks and branches) as these materials would have larger effects on the MISR observation at larger view zenith angles.

### *5.6. Background reflectivity in RGB color composite*

Fig. 8(a) shows a RGB color composite of a MISR BRF mosaic of the study area acquired in spring and Fig. 8(b) shows a color composite of the background reflectivity of the same mosaic. Both color composites show only the forest area in the study region in false color (RGB: NIR, Red and Green). According to Cihlar et al. (1997) the northern belt of the forest is mostly low density coniferous and burnt forests, the middle belt is dense coniferous forest, and the southern part is deciduous and mixed forests. As the images were acquired during early spring the northern part of the forest is in white due to the influence of snow, the southern part is in bright brown because no foliage were on trees, and the evergreen coniferous forest in the middle is in bright red color. The areas covered by coniferous forest, which are in bright red color in Fig. 8(a), are light red in Fig. 8(b), suggesting that the background of the coniferous forest had similar signatures to that of moss/grassland. The spatial variations in the background that can be seen in Fig. 8(b) are not visible in Fig. 8(a). The spatial variations in the background could be analyzed and classified to produce background map if proper training sample and enough field data about the background properties are available. Further studies may be possible to discriminate the background type based on the retrieved background optical properties.

## 6. Discussion

As this study handles a complex issue and to our knowledge this is the first attempt made to retrieve background reflectance from spacebone imageries, it is obvious to start with simple methodology that requires assumptions in order to aid the understanding of the complex issue. Therefore in this study a number of assumptions were made to find the feasibility to retrieve background reflectance from MISR data.

In the methodology, the assumption that the shaded reflectivities of tree crown and the background are comparatively small and approximately equal ($R_{ZT}=R_{ZG}=R_Z$) was made to reduce the unknown parameters in the model. The values 0.002 and 0.08 were given to $R_Z$ for visible and NIR wavelengths, respectively based on the knowledge gained from the Four-Scale simulations. For NIR this value may vary slightly and it is related to the strengths of sky irradiance and the multiple scattering of light in the canopy that is influenced by LAI. In future studies they can also be determined using look-up-tables from the Four-Scale model, although they have secondary importance in determining the background reflectivity.

In retrieving the background reflectivity, two main types of forests were separated, and the accuracy of the retrieval is

therefore depended on the Canada 2000 landcover map. The given architectural parameters of the coniferous and deciduous forests for the Four-Scale model to estimate $P_T$ and $P_G$ are general for the large study area that are covered by the forest with different structures and mixtures. The retrieval results may be improved if the architectural parameters of the forest were given based on detailed forest classes representing different forest structures. It is also possible to expand the study to other types of vegetations if the architectural parameters of various types of vegetation are available for producing look-up-tables.

Here the background reflectivity was estimated assuming the background is Lambertian. The ideal Lambertian surface radiates or reflects equally in all direction (Pradhan, 2001), thus the reflectance in a given spectral band obtained at all viewing geometries will be identical. Most surfaces in nature are non-Lambertian (anisotropic) and different surfaces exhibit different degrees of anisotropy that could be explained using anistropic index (Sandmeier & Deering, 1999). Though the forest background is not an ideal Lambertian surface, the field reflectance measurements of background surface types such as soil, grass, moss and the mixed surface contain heather, blueberry, lingonberry, moss, grass and litter that are given in Peltoniemi et al. (2005) and Pradhan (2001) show low anisotropic index (closer to Lambertian surfaces). An increase in soil moisture increases the anisotropy effect of soil (Pradhan, 2001) might have some influence in the temporal pattern of the background reflectivity (Fig. 6) that explains greening process. For forests with thick understoreys, a complete bidirectional reflectance distribution function (BRDF) has been constructed with Four-Scale model (Leblanc et al., 1999). To apply this BRDF against the underlying soil/moss surface, the understorey density needs to be estimated and this would be another refinement to be made in future studies. Devising a fixed BRDF, as the case for grassland applications (Chopping et al., 2003), would not improve much the accuracy of optical property retrieval for complex backgrounds under forests.

The results from this study are encouraging as the reflectivity values of the forest background during summer tallies with the field measurements given in Peltoniemi et al. (2005). But it is difficult to do detailed comparison without knowing the background type and actual measurements for each type. Background types could vary with different vegetation cover types (Sandmeier & Deering, 1999), and they need to be studied in further detail. In this study the comparison with open grassland was made based on the fact that the grass is one of the predominant background components. Although validation using ground observation is generally difficult for large areas in coarse resolutions, high-resolution airborne measurements would be a useful way to validate our algorithm.

## 7. Conclusion

Multi-angle remote sensing can be a very useful way to characterize ecosystems not only for the forest canopy but also for the underlying background. The MISR data provides bidirectional reflectance of forest canopies in an oblique plane relative to the sun and indicates the hotspot and the darkspot behavior of the forest canopies as well as the influence of the background to the bidirectional reflectance. The Four-Scale model has proven its ability to run with fixed general parameters to quantify the probabilities of viewing illuminated tree crown and background for estimating the background reflectivity. As expected, in summer, the background reflectivities in red and NIR showed greening processes and that are closer to the growing pattern of adjacent grasslands. More precise result could be achieved when the more detail parameters are available for each vegetation cover type. The color composite of background reflectivity is an interesting outcome and this can be used to classify the background component of a forest pixel. The classification of a background image requires systematic ground information and further studies may be possible to classify rock, soil, grass, moss, bush, water, etc. based on retrieved optical properties of the background. When this additional background information is combined with the conventional multispectral remote sensing data, the accuracy of mapping biophysical parameters for terrestrial ecosystems can be greatly improved, and therefore, this use of multiple angle data can eventually help to address key issues of the spatial distribution of vegetation productivity and the impact of climate change on the global terrestrial carbon budget.

## Acknowledgements

We are grateful for the use of processed MISR reflectance and LAI data used in this study. Dr. Dave Diner and his team provided useful instruction manuals and technical assistance that made our work possible. This research was funded by a Discovery Grant to Prof. Jing Chen from the Natural Science and Engineering Council of Canada.

## References

Bothwell, G. W., Hansen, E. G., Vargo, R. E., & Miller, K. C. (2002). The Multi-angle Imaging SpectroRadiometer science data system, its products, tools and performance. *IEEE Transactions on Geoscience and Remote Sensing*, *40*, 1467−1476.

Chen, J. M., & Leblanc, S. G. (1997). A four-scale bidirectional reflectance model based on canopy architecture. *IEEE Transactions on Geoscience and Remote Sensing*, *35*, 1316−1337.

Chen, J. M., & Leblanc, S. G. (2001). Multiple-scattering scheme useful for geometric optical modeling. *IEEE Transactions on Geoscience and Remote Sensing*, *39*, 1061−1071.

Chen, J. M., Ju, W., Cihlar, J., Price, D., Liu, J., Chen, W., et al. (2003a). Spatial distribution of carbon sources and sinks in Canada's forests based on remote sensing. *Tellus. Series B, Chemical and Physical Meteorology*, *55*(2), 622−642.

Chen, J. M., Liu, J., Leblanc, S. G., Lacaze, R., & Roujean, J. -L. (2003b). Multi-angular optical remote sensing for assessing vegetation structure and carbon absorption. *Remote Sensing of Environment*, *84*, 516−525.

Chen, J. M., Menges, C. H., & Leblanc, S. G. (2005). Global mapping of foliage clumping index using multi-angular satellite data. *Remote Sensing of Environment*, *97*, 447−457.

Chopping, M. J., Rango, A., Havstad, K. M., Schiebe, F. R., Ritchie, J. C., Schmugge, T. J., et al. (2003). Canopy attributes of desert grassland and transition communities derived from multiangular airborne imagery. *Remote Sensing of Environment*, *85*, 339−354.

Cierniewski, J., Gdala, T., & Karnieli, A. (2004). A hemispherical-directional reflectance model as a tool for understanding image distinctions between

cultivated and uncultivated bare surfaces. *Remote Sensing of Environment*, *90*, 505−523.

Cihlar, J., Beaubien, J., Xiao, Q., Chen, J., & Li, Z. (1997). Land cover of the BOREAS region from AVHRR and Landsat data. *Canadian Journal of Remote Sensing*, *23*, 164−175.

Deering, D. W., Eck, T. F., & Banerjee, B. (1999). Characterization of the reflectance anisotropy of three boreal forest canopies in spring–summer. *Remote Sensing of Environment*, *67*, 205−229.

Diner, D. J., Asner, G. P., Davies, R., Knyazikhin, Y., Muller, J. P., Nolin, A. W., et al. (1999). New directions in Earth observing: Scientific applications of multi-angle remote sensing. *Bulletin of the American Meteorological Society*, *80*, 2209−2228.

Diner, D. J., Beckert, J. C., Bothwell, G. W., & Rodriguez, J. I. (2002). Performance of the MISR instrument during its first 20 months in Earth orbit. *IEEE Transactions on Geoscience and Remote Sensing*, *40*, 1449−1466.

Diner, D. J., Beckert, J. C., Reilly, T. H., Bruegge, C. J., Conel, J. E., Kahn, R. A., et al. (1998). Multi-angle Imaging SpectroRadiometer (MISR) instrument description and experiment overview. *IEEE Transactions on Geoscience and Remote Sensing*, *36*, 1072−1087.

Field, C. B., Raupach, M. R., & Victoria, R. (2003). The global carbon cycle: Integrating humans, climate and the natural world. In C. B. Field & M.R. Raupach (Eds.), *The global carbon cycle: Integrating humans, climate and the natural world* (pp. 1−13). Washington, D.C.: Island Press.

Gao, F., Schaaf, C. B., Strahler, A. H., Jin, Y., & Li, X. (2003). Detecting vegetation structure using a kernel-based BRDF model. *Remote Sensing of Environment*, *86*, 198−205.

Gemmell, F. (2000). Testing the utility of multi-angle spectral data for reducing the effects of background spectral variations in forest reflectance model inversion. *Remote Sensing of Environment*, *72*, 46−63.

Gobron, N., Pinty, B., Verstraete, M. M., Widlowski, J., & Diner, D. J. (2002). Uniqueness of multiangular measurements—Part II: Joint retrieval of vegetation structure and photosynthetic activity from MISR. *IEEE Transactions on Geoscience and Remote Sensing*, *40*, 1574−1592.

Hese, S., Lucht, W., Schmullius, C., Barnsley, M., Dubayah, R., Knorr, D., et al. (2005). Global biomass mapping for an improved understanding of the $CO_2$ balance—The Earth observation mission Carbon-3D. *Remote Sensing of Environment*, *94*, 94−104.

Hu, J., Tan, B., Shabanov, N., Crean, K. A., Martonchik, J. V., Diner, D. J., et al. (2003). Performance of the MISR LAI and FPAR algorithm: A case study in Africa. *Remote Sensing of Environment*, *88*, 324−340.

Jovanovic, V. M., Smyth, M. M., Zong, J., Ando, R., & Bothwell, G. W. (1998). MISR photogrammetric data reduction for geophysical retrievals. *IEEE Transaction on Geoscience and Remote Sensing*, *36*, 1290−1301.

Knyazikhin, Y., Martonchik, J. V., Diner, D. J., Myneni, R. B., Vertraete, M., Pinty, B., et al. (1998). Estimation of vegetation canopy leaf area index and fraction of absorbed photosynthetically active radiation from atmosphere-corrected MISR data. *Journal of Geophysical Research*, *103*, 32239−32356.

Leblanc, S. G., Bicheron, P., Chen, J. M., Leroy, M., & Cihlar, J. (1999). Investigation of directional reflectance in boreal forests with an improved 4-scale model and airborne POLDER data. *IEEE Transaction on Geoscience and Remote Sensing*, *37*, 1396−1414.

Leblanc, S. G., Chen, J. M., White, H. P., Latifvic, R., Roujean, J. R., & Lacaze, R. (2005). Canada-wide foliage clumping index mapping from multi-angular POLDER measurements. *Canadian Journal of Remote Sensing*, *31*, 364−376.

Li, X., & Strahler, A. H. (1985). Geometric optical modeling of a coniferous forest canopy. *IEEE Transactions on Geoscience and Remote Sensing*, *23*, 705−721.

Liu, J., Chen, J. M., Cihlar, J., & Chen, W. (1999). Net primary productivity distribution in the BOREAS region from a process model using satellite and surface data. *Journal of Geographical Research*, *104*, 27735−27754.

Nolin, A. W. (2004). Towards retrieval of forest cover density over snow from the Multi-angle Imaging SpectroRadiometer (MISR). *Hydrological Processes*, *18*, 3623−3636.

Peddle, D. R., Hall, F. G., & LeDrew, E. F. (1999). Spectral mixture analysis and geometric-optical reflectance modeling of boreal forest biophysical structure. *Remote Sensing of Environment*, *67*, 288−297.

Peltoniemi, J. I., Kaasalainen, S., Naranen, J., Rautianinen, M., Stengerg, P., Smolander, H., et al. (2005). BRDF measurement of understory vegetation in pine forests: Dwarf shrubs, lichen, and moss. *Remote Sensing of Environment*, *94*, 343−354.

Potter, C., Klooster, S., Steinbach, M., Tan, P., Kumar, V., Shekhar, S., et al. (2003). Global teleconnections of climate to terrestrial carbon flux. *Journal of Geographical Research*, *108*, D17.

Pradhan, P. S. (2001). *Measuring the effects of soil parameters on bidirectional reflectance distribution function*. Master thesis report, Department of electrical and computer engineering, Mississippi State University, Mississippi.

Rautiainen, M., Stenberg, P., Nilson, T., & Kuusk, A. (2004). The effect of crown shape on the reflectance of coniferous stands. *Remote Sensing of Environment*, *89*, 41−52.

Sandmeier, St., & Deering, D. W. (1999). Structure analysis and classification of boreal forests using airborne hyperspectral BRDF data from ASAS. *Remote Sensing of Environment*, *69*, 281−295.

Treitz, P. M., & Howarth, P. J. (1999). Hyperspectral remote sensing for estimating biophysical parameters of forest ecosystems. *Progress in Physical Geography*, *23*, 359−390.

Verstraete, M. M., Pinty, B., & Myneni, R. (1996). Potential and limitation of information extraction on the terrestrial biosphere from satellite remote sensing. *Remote Sensing of Environment*, *58*, 201−214.

White, P. H., Miller, J. R., & Chen, J. M. (2001). Four-scale linear model for anisotropic reflectance (FLAIR) for plant canopies—Part I: Model description and partial validation. *IEEE Transactions on Geoscience and Remote Sensing*, *39*, 1073−1083.

Zhang, Y., Shabanov, N., Knyazikhin, Y., & Myneni, R. B. (2002b). Assessing the information content of multiangle satellite data for mapping biomes: II. Theory. *Remote Sensing of Environment*, *80*, 435−446.

Zhang, Y., Tian, Y., Myneni, R. B., Knyazikhin, Y., & Woodcock, C. E. (2002a). Assessing the information content of multiangle satellite data for mapping biomes: I. Statistical analysis. *Remote Sensing of Environment*, *80*, 418−434.